Environ. Sci. Technol. **1999**, *33,* 3160−3165

Manganese Dioxide as a Catalyst for Oxygen-Independent Atrazine Dealkylation

DAOJING WANG,[†] JIN Y. SHIN,[‡] MARCOS A. CHENEY,*[,‡] GARRISON SPOSITO,[§] AND THOMAS G. SPIRO*[,†]

Department of Chemistry, Princeton University, Princeton, New Jersey 08544-1009, Department of Environmental Science, Cook College, Rutgers University, New Brunswick, New Jersey 08901-8551, and Earth Sciences Division, Lawrence Berkeley National Laboratory, University of California, Berkeley, California 94720

The herbicide atrazine is widely distributed in the environment, and its reactivity with soil minerals is an important issue. We have studied atrazine degradation on the surface of synthetic hydrous (10% H_2O) δ-MnO_2 (birnessite) using UV resonance Raman spectroscopy and gas chromatography. The products are mainly mono- and didealkyl atrazine. Atrazine disappearance is rapid ($\tau_{1/2} \sim 5$ h at 30 °C), independent of whether O_2 is present or not. MnO_2 reduction is a minor reaction, and the alkyl chains are converted mainly to the alkenes, in a nonredox process. A novel dealkylation mechanism is proposed involving proton transfer to Mn(IV)-stablized oxo and imido bonds. When O_2 is present, olefin oxidation and ring mineralization are also observed as secondary reactions in addition to those discussed above. Thus δ-MnO_2, a common soil constituent, is found to promote efficient N-dealkylation of the herbicide atrazine at 30 °C, via a nonoxidative mechanism.

Atrazine [AT, 6-chloro-*N*-ethyl-*N*′-(1-methylethyl)-1,3,5-triazine-2,4-diamine] along with its degradation product, deethylatrazine [DEA, 6-chloro-*N*-(1-methylethyl)-1,3,5-triazine-2,4-diamine], is the most frequently detected herbicide in shallow groundwater bodies of the United States (*1*). Similar findings hold for soils (*2*) and rainfall (*3*) in the Midwest cornbelt, with major impact on AT loading of the Great Lakes (*4*). This widespread distribution is of particular concern because AT appears to be a potent disrupter of cell chromosome structure (*5*) and estrogen metabolism (*6*).

Atrazine degradation by microbial catalysis in soil environments is a relatively slow process [half-life, 60−100 days (*2, 3*)] which forms the nontoxic products, DEA and deisopropylatrazine [DIA, 6-chloro-*N*-ethyl-1,3,5-triazine-2,4-diamine), or occasionally hydroxyatrazine [HYAT, 6-hydroxy-*N*-ethyl-*N*′-(1-methylethyl)-1,3,5-triazine-2,4-diamine) as well as the corresponding hydrolyzed forms of DEA and DIA (*7*). The preponderance of DEA over DIA after microbial degradation of AT is well-documented (*2, 8*). This asymmetry in the ratio of dealkylated products also is observed in the abiotic degradation reactions of AT by hydroxy radical photolysis mediated by nitrate (*9*). [Direct photolysis produces HYAT and the hydroxylated forms of DEA and DIA (*10*).] Torrents et al. (*9*) have suggested that this dealkylated product asymmetry will occur whenever stereochemistry, as opposed to electron transfer, controls the degradation mechanism.

Abiotic, proton-catalyzed degradation of AT to HYAT on mineral and humus solid surfaces is well-known (*11*−*14*) but limited to conditions of relatively low pH and/or water content in soil environments (*15*). Surface-catalyzed, nonphotochemical oxidation of xenobiotic organic chemicals on metal oxide adsorbents also has been investigated extensively (*16*), but little research has been reported on this mode of abiotic degradation for herbicides (*15*). Cheney et al. (*17*) recently investigated the degradation reactions of AT adsorbed on δ-MnO_2 by applying a combination of calorespirometric and spectroscopic techniques. They identified a complex exothermic process, in the presence of O_2, that produced DEA and DIA in approximately equal amounts over a 12 h reaction at 30 °C. Minor CO_2 evolution and Mn(II) production also were observed over a 48 h period, during which the DEA and DIA products both disappeared. Cheney et al. (*17*) were not able to quantify the subsequent degradation products or to elucidate the mechanism of CO_2 production. Their results, however, did demonstrate the potential for surface-catalyzed degradation of AT on δ-MnO_2 over time scales that are much shorter than those observed for microbiologically mediated degradation and with an equal production (and subsequent loss) of DEA and DIA that contrasts sharply to the product asymmetry in the biotic degradation pathway.

These issues prompted us to carry out a more comprehensive study of the δ-MnO_2-catalyzed reactions of AT using a combination of analytical techniques. In the initial work (*17*), HPLC was incapable of distinguishing one of the monodealkylation products, DIA, from the suspected subsequent didealkylation product, DDA (6-chloro-1,3,5-triazine,-2,4-diamine), thus preventing a mass-balance analysis. We found ultraviolet resonance Raman (UVRR) spectroscopy to be effective in quantitating all three dealkylation products as well as the loss of AT itself. Strikingly, moreover, we find that dealkylation proceeds at the same rate, regardless of whether O_2 is present. A search for the alkyl fragments revealed olefin production, while Mn assays showed negligible release of Mn(II) from the oxide mineral. Thus, the primary reactions appear to involve no net redox reaction (Figure 1). When O_2 is present, some olefin oxidation to ketones and aldehydes and some ring mineralization are observed, but these are minor reactions, in agreement with our earlier observations (*17*).

These findings may have implications for controlling the fate and lifetime of AT in soils. Although the conditions of our laboratory study are quite far from those encountered in the environment, the ability of δ-MnO_2 to catalyze oxygen-independent N-dealkylation of atrazine could shorten AT residence times, and could also affect biodegradation pathways by altering the nature of the substrates available for microbial metabolism. Further studies are required to estimate the importance of the mechanism under natural conditions.

Experimental Section

Synthesis of δ-MnO_2 and the Reaction System. The manganese oxide, δ-MnO_2, was synthesized by the method of McKenzie (*18*) and characterized by X-ray powder diffraction.

* Corresponding authors phone: (609)258-3907 and (732)932-9094; fax: (609)258-0348; e-mail: spiro@chemvax.princeton.edu and cheney@AESOP.Rutgers.edu.

[†] Princeton University.

[‡] Rutgers University.

[§] University of California.

10.1021/es990419t CCC: $18.00
Published on Web 08/07/1999

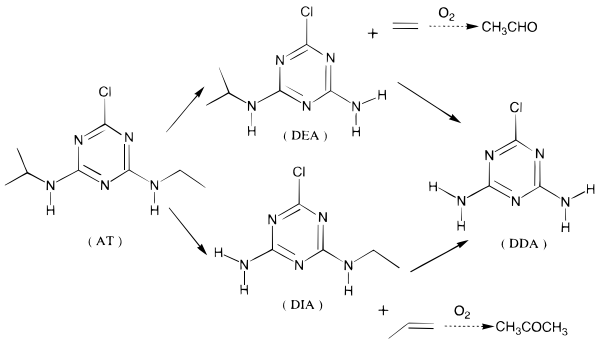

FIGURE 1. Reaction scheme for MnO_2-catalyzed atrazine dealkylation. Secondary reactions with O_2 are indicated by dotted lines.

Birnessite peaks appeared at 0.720, 0.361, and 0.142 nm, in good agreement with the results of Jones and Milne (*19*) for samples of this mineral. The surface area was determined to be 39 m^2/g similar to that reported by McKenzie (*18*), using the BET single point method (Quantachrome Monosorb analyzer). The water content of the MnO_2 was determined to be 10 wt %, from the weight loss upon heating at 110 °C for 5 h.

Exactly 300 mg (3.5 mmol) of δ-MnO_2 were suspended in 3 mL of anhydrous, analytical reagent-grade ethyl ether. Analytical reagent-grade AT (Chem service, Westchester, PA) was dissolved in ethyl ether to make a 10 mM stock solution. As in our previous study (*17*), the basic experiment involves deposition of AT on δ-MnO_2 from diethyl ether solution, low-temperature evaporation of the solvent, and extraction of the sample with methanol, after appropriate incubation intervals at 30 °C. The methanol extracts were examined by UVRR spectroscopy to evaluate dealkylation yields. Volatile products were determined by GC analysis of headspace gas above the samples. The experiment was conducted under N_2 as well as in air. As a control, the same experiment was carried out with alumina instead of δ-MnO_2.

Approximately 300 μL of AT stock solution was added to the δ-MnO_2 suspension to provide initially 3.0 μmol AT for reaction. The suspension was placed in a shaker table for 10 min, after which the solid was then placed in a vacuum desiccator at 0 °C for 3 h. Ethyl ether was removed rapidly under these conditions permitting subsequent investigation of the surface kinetics at 30 °C over a 336 h period. When anaerobic conditions were required, the δ-MnO_2-AT sample mixture was prepared in a Coy Environmental Chamber (Coy Lab. Inc., MI) after introducing N_2 gas and 5% N_2/H_2 gas mixture. Alumina was used as a desiccant to remove moisture inside the chamber. H_2 gas and a Pd catalyst were used to remove O_2 impurities caused by diffusion during normal operating procedures.

After 0, 4, 8, 12, 24, 48, 72, and 96 h reaction at 30 °C in the absence or presence of O_2, the samples were extracted with methanol (extracted twice in succession, with vigorous mixing for 5 min). Quantitation of AT, DEA, DIA, and DDA in the methanol sample extracts was by UVRR spectroscopy.

Duplicate samples of the δ-MnO_2-AT mixture in 2-mL screw top septum vials were prepared in the absence or presence of O_2, incubated at 30 °C in an oven to mimic the UVRR experiments, and then analyzed for reaction products other than AT, DEA, DIA, or DDA. For these reactions, the vial headspace gas (100 μL aliquot) was analyzed after 0 (at laboratory temperature and 30 °C), 24, 48, 72, 96, 120, 144, 168, and 336 h for products such as ethylene, propylene, acetone, and acetaldehyde, using a Shimadzu CR501 series gas chromatograph. Gas samples were passed through a 10 m Alltech (0.18 μm ID) QC345 fused-silica capillary column into a thermal conductivity detector. Outflow from the detector was then passed through a 15 m, 80−100 mesh 5 AMS column and into a second thermal conductivity detector. A Model CR501 Chromatopac integrator was used to determine peak areas.

Detection of Mn. Mixtures of AT and δ-MnO_2 were incubated at 30 °C to mimic a standard experimental run. At 4, 12, 24, 36, 50, 75, 100, and 160 h, triplicate samples (300 mg each) of these mixtures were extracted with 3 mL of methanol to quench the reaction. The suspension then was filtered, and the solid was extracted again by shaking overnight with 10 mL of 0.03 M HCl/0.03 M H_2SO_4 mixture [modified Mehlich-1 method (*20*)]. Methanol was evaporated, and the residue was combined with the acidified extract for analysis. Untreated δ-MnO_2 was used as a control. Manganese analysis in the extracts was performed on a Perkin-Elmer Model 4100 ZL graphite furnace atomic absorption spectrophotometer.

UV Resonance Raman Spectroscopy. UVRR spectra were obtained with a 1.26 m single-stage spectrometer (SPEX 1269) with an intensified diode array multichannel detector (*21*). Laser excitation at 229 nm was provided by a frequency-doubled Innova 300 argon ion laser (Coherent). The laser power at the sample was about 0.35 mW. The scattered light was collected with an f/1 paraboloid mirror in backscattering geometry and focused with an f-matching lens. The reaction extracts were contained in a 5 mm quartz EPR tube which was spun around a stationary helical wire. Cooled N_2 gas kept the sample temperature between 10 and 15 °C. Spectral acquisition was carried out in 5 min increments. No photoproducts were observed under these conditions, as verified by comparison of the UVRR spectra of the same sample at 5 s intervals.

A least-squares method for spectral analysis (Labcalc) was employed to quantify the products. Methanol, which was used as the extraction solvent, has a very strong band at 1034 cm^{-1}, well-separated from the Raman bands of the AT degradation products. This band was used as an internal intensity standard. After the Raman intensity was calibrated, the UVRR spectrum of methanol was subtracted from the experimental spectra digitally. The calibration file for the quantification was generated from the spectral matrix of standard solutions of pure AT, DEA, DIA, and DDA as well as their mixtures. The least-squares fit was generated for 12 points, corresponding to peak wavenumbers: 900, 914, 930, 962, 1050, 1368, 1417, 1517, 1526, 1582, and 1614 cm^{-1}. The uncertainty in the resulting concentration estimates was within ±5%.

Results

Figure 2 shows UVRR spectra (excitation wavelength, 229 nm) of AT, DEA, DIA, and DDA at 1 mM concentration in methanol. Atrazine and its dealkylation products absorb strongly in the ultraviolet region, and the $\pi-\pi^*$ electronic transitions resonantly enhance a series of vibrational modes of the aromatic ring which are sensitive to alkyl substituents (Figure 1). The enhancement pattern differs markedly among AT and its dealkylation products, and the overall enhancement decreases systematically with dealkylation: the 229 nm excitation wavelength is further from resonance as the absorption band maximum in methanol shifts from 223 nm for AT, to 216 nm for DIA and DEA, and to 210 nm for DDA. The two monodealkylated products, DEA and DIA, give similar UVRR spectra, but there are clear spectral differences in the 900−1000 cm^{-1} region that permit reliable quantitation. For example separable peaks are seen at 962, 900, 930, and 914 cm^{-1} for AT, DEA, DIA, and DDA, respectively. Moreover, there are numerous differences in band intensities throughout the spectra. The ability to resolve spectral components made UVRR the preferred method of reaction monitoring, because of the difficulty of resolving DEA and DIA peaks via HPLC (*17*).

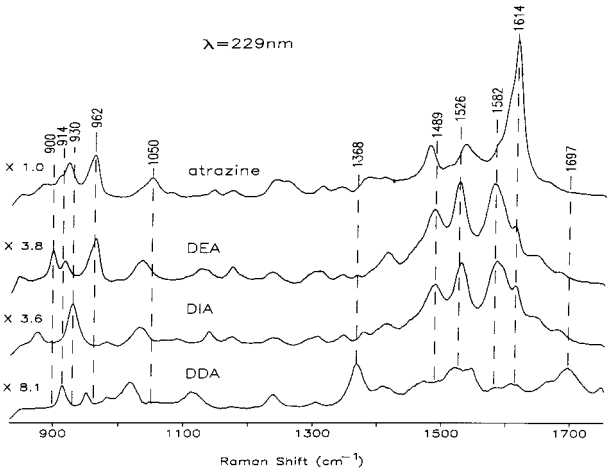

FIGURE 2. Reference UVRR spectra for AT and its dealkylation products (1 mM in methanol). Scale factors are indicated for the normalized intensity using the 1034 cm^{-1} solvent band (methanol) as a reference. This band has been subtracted digitally. The intensities are lower for DEA and DIA than AT, and lower still for DDA, because their absorption maxima are blue-shifted from the 229 nm excitation wavelength.

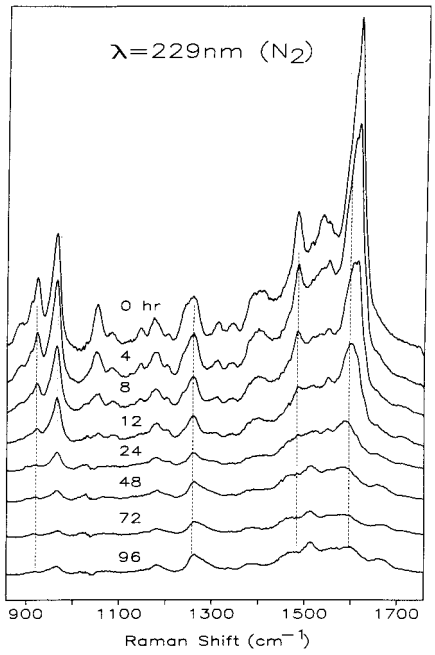

FIGURE 3. UVRR spectra for methanol extracts of AT/MnO_2 samples at the indicated incubation times (30 °C) under N_2. The AT peaks are progressively replaced by weaker peaks from dealkylation products. Methanol solvent peaks have been subtracted digitally.

Figure 3 shows UVRR spectra of the methanol extracts from AT-δ-MnO_2 mixtures obtained after increasing reaction time at 30 °C under N_2. The progressive loss of intensity and the peak shifts reflect the loss of AT and its replacement by dealkylation products. The mixtures were quantitated via deconvolution of the spectra into those of the four components in Figure 1. The time-course of the extract composition is shown in Figure 4 for samples incubated under N_2. There is an approximately first-order decrease in AT ($\tau_{1/2} \sim 5$ h) and a corresponding increase in dealkylation products: first the monodealkylated triazines, in nearly equal amounts, and then DDA. The former reach maxima at 12 h and then decline (albeit at a slower rate than AT) as they are further dealkylated. The dealkylation products account almost quantitatively for the lost AT, as indicated by the top trace in Figure 3, which shows the total moles of AT plus degradation products. This total declined by only 10% over the 96 h of the experiment. Thus, the AT ring remained intact, and degradation was limited almost exclusively to dealkylation.

The time-course of extract composition for the experiment performed in the presence of O_2 (ambient atmosphere) is shown in Figure 5. The data for AT loss and DEA/DIA increase are very similar to those reported by Cheney et al. (*17*), whose CO_2 evolution results are superposed. The top trace in the figure now accounts for only 70% of the reactant and spectrally quantitated products. We infer that the remaining 30% was lost to mineralization, and, indeed, the CO_2 yield from the earlier study (*17*) accounts for most of the deficit. Significantly, however, the rate of AT disappearance is almost the same in the presence of O_2 as in its absence. Thus, the initial reaction is oxygen-independent dealkylation, but, when O_2 is present, the products are slowly oxidized and mineralized.

There was no evidence for replacement of the ring Cl by OH under our reaction conditions. This substitution would have affected the UVRR spectra substantially. A search for HYAT via HPLC was also negative (data not shown). To assess the essential role of δ-MnO_2, we ran a control with AT deposited on alumina under the same conditions of incubation and extraction. The UVRR spectrum of AT was unaltered over a period of 48 h (data not shown).

Gas chromatographic analysis of the reaction vessel headspace gave positive results for ethylene and propylene, and an increasing time-course was observed (Figure 6). However, only a small fraction of the olefin molecules reached the gas phase. To obtain the results in Figure 6, 60 °C was required. But the yields were much lower than stoichiometric (compare ordinates for Figures 4 and 6), and they continued to climb long after the dealkylation product yields had leveled off (Figure 4). Thus, only a fraction of the olefin products accumulated in the vapor phase, and, because of slow desorption, this fraction lagged behind the production rate. Consistent with this interpretation, the propylene yields were only half the ethylene yields, even though the yields of DIA and DEA were the same (Figure 4). [Ethylene is expected to volatilize more readily than propylene]. In a control experiment, pure AT was heated at 60 °C, and no degradation was detected.

When O_2 was present in the reaction vessel, similar yield curves were obtained for ethylene and propylene (Figure 7). In addition, acetaldehyde and acetone were detected in the headspace, and their yields also increased with time, but with a distinct lag period relative to ethylene and propylene. Therefore, it seems likely that the carbonyl compounds resulted from oxidation of the olefins after the dealkylation reactions had occurred. Since the dealkylation yields and their time-course were unaffected by O_2 (Figures 4 and 5), carbonyl production should have lowered the olefin yields stoichiometrically. This was not observed, probably because desorption from the oxide surface is the rate-controlling process. Although they are not subject to resonance enhancement at 229 nm, acetaldehyde and acetone were also detected in the UVRR spectra of the sample extracts via their isolated carbonyl bands at 1708 and 1718 cm^{-1} (Figure 8), but only when O_2 was present in the reaction vessel.

After the AT and reaction products were extracted with methanol, the MnO_2 phase was assayed for soluble Mn using acid extraction and graphite furnace AAS. Only traces were observed (Figures 6 and 7). The presence of O_2 had almost no effect on Mn yield. The yield increased at first and then declined, suggesting that traces of Mn^{2+} in the original birnessite are slowly released under the extraction conditions.

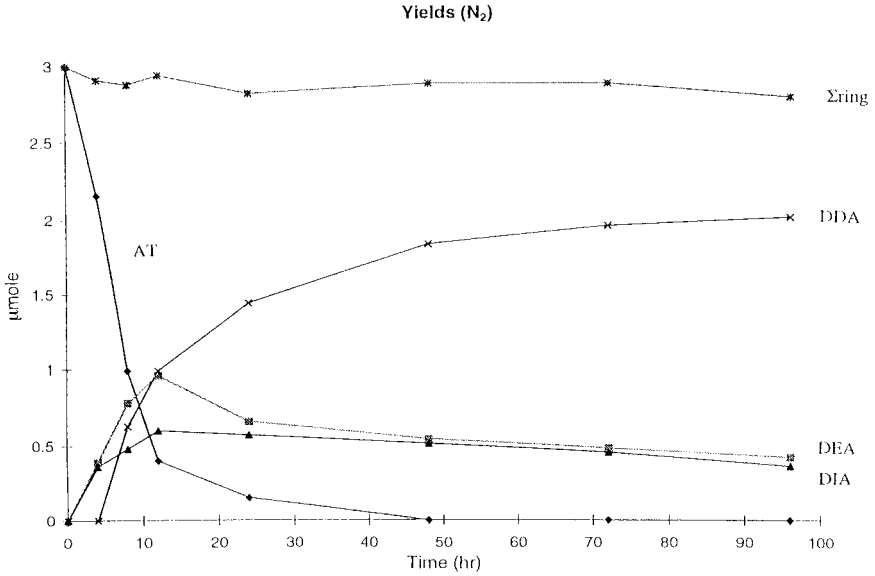

FIGURE 4. Reaction-progress curves for the AT/MnO_2 extracts under N_2 based on deconvolution of the UVRR spectra in Figure 2. Yields were calculated from the spectral intensity using the methanol 1034 cm^{-1} peak as an internal standard. The top trace (Σring) is the sum of yields of the dealkylation products and AT, showing near-quantitative preservation of the triazine ring.

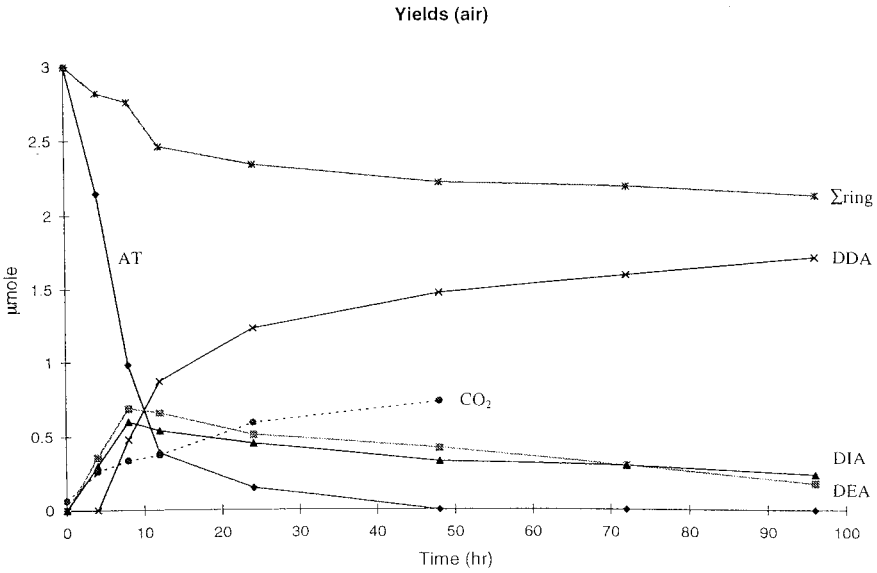

FIGURE 5. As in Figure 3, but for samples reacted in contact with air. The CO_2 yields, taken from a similar experiment reported previously (*17*), show that loss of the triazine ring results mainly in mineralization to CO_2.

Discussion

The most striking result in the present study is that the rate of AT disappearance at the δ-MnO_2 surface does not depend on the presence of O_2. It might have been expected that AT is degraded by MnO_2 catalysis of oxidation by O_2, but this is not the case. Atrazine is efficiently dealkylated regardless of whether O_2 is present. In the absence of O_2, dealkylation accounts almost quantitatively for AT disappearance, but, in the presence of O_2, there is some mineralization of the AT ring, ca. 30% over 96 h. Thus, O_2 cannot be involved in the mechanism of the dealkylation reaction but only in secondary oxidation. Dealkylation is equally rapid for the ethyl and isopropyl substituents on the triazine ring, and the DDA product results from subsequent dealkylation of the monodealkyl products at about the same rate (Figures 4 and 5).

Upon dealkylation, the ethyl and isopropyl groups are converted to ethylene and propylene. Although a mass balance was not obtained because of slow volatilization of the olefins from the solid surface, the progressive time-course of the GC yield curves (Figures 6 and 7) leaves little doubt that olefins were the primary dealkylation products. Some oxidation to the corresponding carbonyl compounds was detectable but only in the presence of O_2 and only with a lag following olefin production (Figure 7). We conclude that side chain oxidation was after the primary dealkylation reaction which produced olefin products.

The oxide mineral δ-MnO_2 is a well-known solid oxidant, and its surface redox reactions with xenobiotic organic chemicals have been studied extensively (*16*). The oxidation of anilines and phenols (*22*), for example, has been characterized under environmentally relevant conditions. However, alkylamine substituents on AT are deactivated with respect to oxidation because electron density is withdrawn from them by the chlorine-bearing triazine ring (*23*). The inability of δ-MnO_2 to oxidize AT is seen by the fact that only traces of reduced Mn were detected in the acid extracts, and the Mn yield does not follow the time course of AT disappearance. While it is possible that lower valent Mn

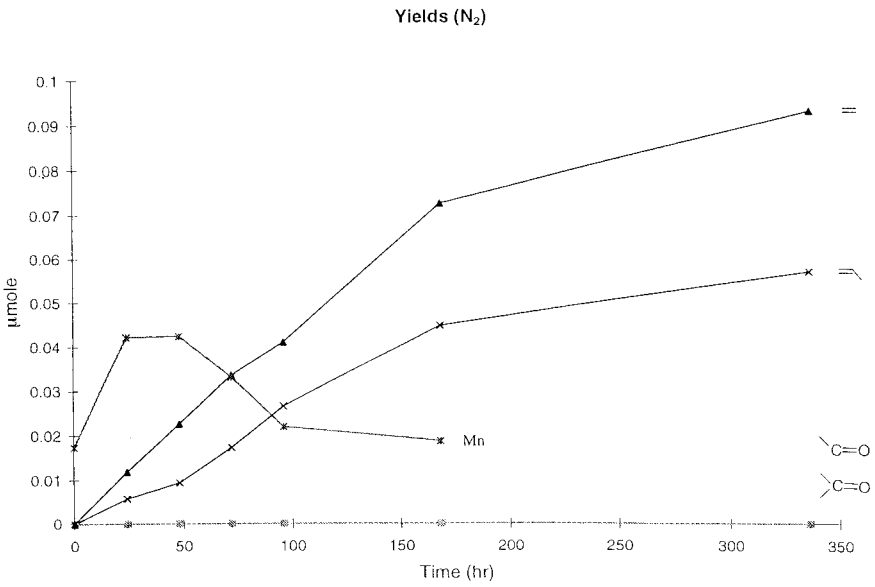

FIGURE 6. Reaction-progress curve for anaerobic ethylene and propylene production in the sample headspace, after 10 min heating at 60 °C, as detected by GC. Also shown is the yield of total Mn in the sample extracts, detected by AAS. No acetaldehyde and acetone were detected.

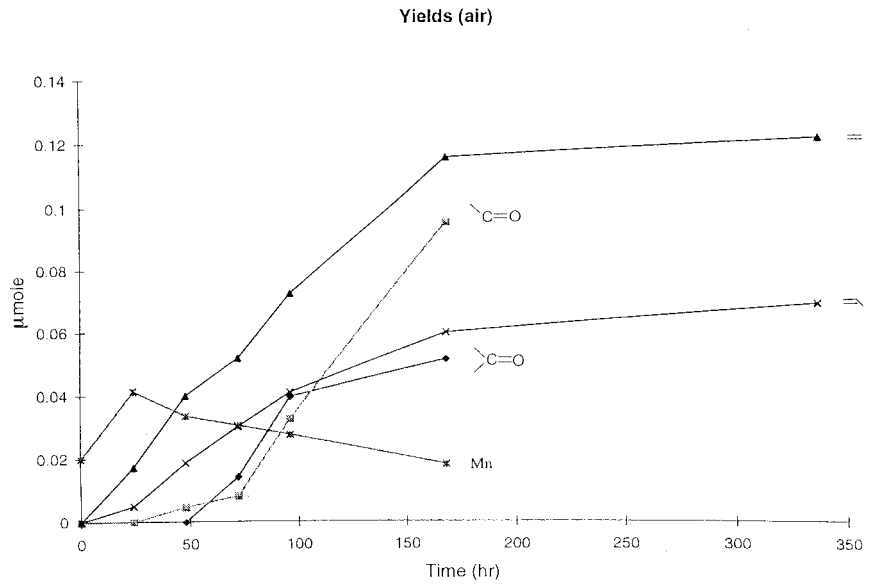

FIGURE 7. As in Figure 5, but for samples exposed to air (O_2). Acetaldehyde and acetone were measured simultaneously by GC.

remained trapped in the MnO_2 lattice, the HCl extraction procedure (*20*) is generally considered to be a reliable method for estimating MnO_2 reduction. Dealkylation to olefin products does not involve oxidation or reduction of AT. Yet δ-MnO_2 is not an inert substrate for the reaction, because the alumina control was completely unreactive, even with O_2 present.

What characteristic of δ-MnO_2 would permit it to catalyze dealkylation with no net redox reaction? We believe that the key lies in the ability of Mn(IV) to form double bonds with O or N ligands by accepting π electrons into empty d orbitals (*24*). These double bonds are of intermediate strength, because the d^3 configuration of Mn(IV) limits the π-acceptor ability. Consequently, the O or N donor atoms remain basic and can engage in proton-transfer reactions. A pair of such transfers can provide a convenient mechanism for AT dealkylation, as illustrated in Figure 9. Manganese(IV) in the oxide structure can coordinate to N in one of the amine substituents via its lone pair. Surface Mn(IV) have terminal oxo ligands which can then attract a proton from the β-carbon of the N-bound alkyl group. Subsequent β-elimination of the olefin is promoted by imido N═Mn(IV) double bond formation. The −HN═Mn−OH fragment then rearranges to $-H_2N-Mn{=}O$, and dissociation of the bound amine completes the dealkylation reaction. Thus electrons and protons are shuttled transiently via the Mn(IV) with no net redox.

This reaction proceeds rapidly, irrespective of whether O_2 is present, but O_2 does induce slower oxidation reactions, producing the carbonyl derivatives of the olefins and ring opening with CO_2 production. A possible mechanism would be interception by O_2 of one of the intermediate structures in Figure 9, with subsequent rearrangements of the resulting peroxy radical. If this were the case, then a fraction of the AT would be channeled into oxidation pathways. However, the yield curves show a definite lag between olefin production and carbonyl production (Figure 7). Consequently, the olefin- and carbonyl-yielding reactions do not have a common intermediate. We speculate that the olefin must be oxidized in a subsequent step, possibly involving a surface complex of olefin and O_2.

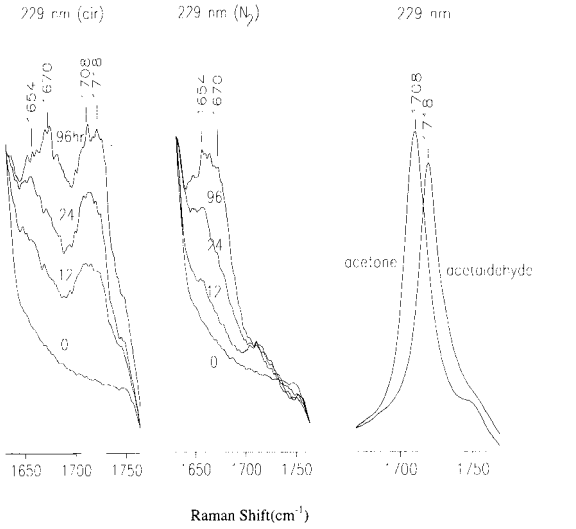

FIGURE 8. Expanded view of UVRR spectra, for aerobic and anaerobic samples, showing the growth of carbonyl bands from acetone (1708 cm^{-1}) and acetaldehyde (1718 cm^{-1}) (right panel) for the aerobic samples. The 1654 and 1670 cm^{-1} peaks are from AT dealkylation products. Incubation times (hours) are indicated.

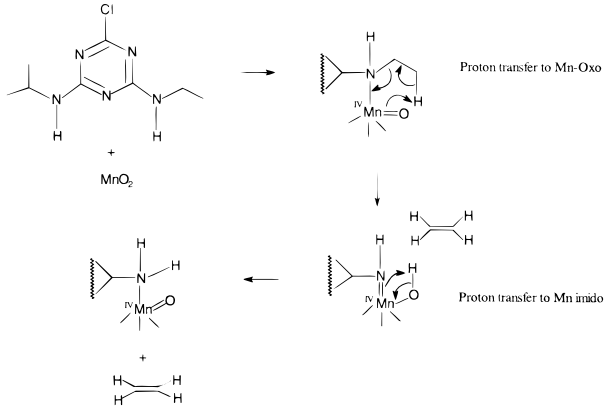

FIGURE 9. Proposed mechanism for AT dealkylation with no net oxidation or reduction.

Further studies are needed to determine the extent to which MnO_2-catalyzed AT dealkylation can occur in the environment. Many parameters are likely to affect the reaction rate. The soil water content is likely to be a critical variable because of competition between AT and water for MnO_2 adsorption sites. Anhydrous conditions are not required, since our δ-MnO_2 was 10% hydrous. Preliminary data (unpublished) indicate that AT reactivity is inhibited at significantly higher water contents for birnessite but not necessarily for other MnO_2 preparations. The role of water and of the MnO_2 surface characteristics will be addressed in future work.

Acknowledgments

The research reported herein was supported in part by the Director, Office of Energy Research, Office of Basic Energy Sciences, Geosciences Program, of the U.S. Department of Energy under Contract No. DE-AC03-76SF00098 and DE-FG02-97ER14755, and in part by the Agricultural Experiment Station, Cook College, Rutgers University. The UVRR Raman facility at Princeton is supported by NIH Grant GM22576 from the National Institute of General Medical Sciences.

Literature Cited

(1) Kolpin, D. W.; Barbash, J. E.; Gilliom, R. J. *Environ. Sci. Technol.* **1998**, *32*, 558−566.
(2) *Herbicide Metabolites in Surface Water and Groundwater*; Meyer, M. T., Thurman, E. M., Eds.; ACS Symposium Series 630; American Chemical Society: Washington, DC, 1996; 318 pp.
(3) Goolsby, D. A.; Thurman, E. M.; Pomes, M. L.; Meyer, M. T.; Battaglin, W. A. *Environ. Sci. Technol.* **1997**, *31*, 1325−1333.
(4) Schottler, S. P.; Eisenreich, S. J. *Environ. Sci. Technol.* **1994**, *28*, 2228−2232.
(5) Biradar, D. P.; Rayburn, A. L. *J. Environ. Qual.* **1995**, *24*, 1222−1225.
(6) Patlak, M. *Environ. Sci. Technol.* **1996**, *30*, 210A−211A.
(7) Koskinen, W. C.; Conn, J. S.; Sorenson, B. A. In *Herbicide Metabolites in Surface Water and Groundwater*; Meyer, M. T., Thurman, E. M., Eds.; ACS Symposium Series 630; American Chemical Society: Washington, DC, 1996; pp 125−139.
(8) Kruger, E. L.; Rice, P. J.; Anhalt, J. C.; Anderson, T. A.; Coats, J. R. *J. Environ. Qual.* **1997**, *26*, 95−101.
(9) Torrents, A.; Anderson, B. G.; Bilboulian, S.; Johnson, W. E.; Hapeman, C. J. *Environ. Sci. Technol.* **1997**, *31*, 1476−1482.
(10) Pelizetti, E.; Maurino, V.; Minero, C.; Carlin, V.; Pramauro, E.; Zerbinati, O.; Tosato, M. L. *Environ. Sci. Technol.* **1990**, *24*, 1559−1565.
(11) Felbeck, G. T.; Li, G.-C. *Soil Sci.* **1972**, *114*, 201−209.
(12) Armstrong, D. E.; Konrad, J. G. In *Pesticides in Soil and Water*; Guenzi, W. D., Ed.; Soil Science Society of America: Madison, WI, 1974; pp 123−131.
(13) Gamble, D. S.; Khan, S. U. *Can. J. Chem*. **1992**, *70*, 1597−1603.
(14) Evangelou, V. P.; Wang, J. *Spectrochim. Acta* **1993**, *49A*, 291−295.
(15) Wolfe, N. L.; Mingelgrin, U.; Miller, G. C. In *Pesticides in the Soil Environment: Processes, Impacts, and Modeling*; Cheng, H. H., Ed.; Soil Science Society of America: Madison, WI, 1990; pp 103−168.
(16) Stone, A. L.; Godtfredsen, K. L.; Deng, B. In *Chemistry of Aquatic Systems: Local and Global Perspectives*; Bidoglio, G., Stumm, W., Eds.; Kluwer Academic: Boston, MA, 1994; pp 337−374.
(17) Cheney, M. A.; Shin, J. Y.; Crowley, D. E.; Alvey, S.; Malengreau, N.; Sposito, G. *Colloids Surf.* **1998,** in press.
(18) McKenzie, R. M. *Mineral. Magn*. **1971**, *38*, 493−502.
(19) Jones, L. H. P.; Milne, A. A. *Mineral. Magn*. **1956**, *31*, 283−286.
(20) Gambrell, R. P. In *Methods of Soil Analysis. Part*—Chemical Methods; Sparks, D. L., Ed.; Soil Science Society of America: Madison, WI, 1996; pp 665−682.
(21) (a) Su, C.; Wang, Y.; Spiro, T. G. *J. Raman Spectrosc.* **1990**, *21*, 435. (b) Asher, S. A.; Bormett, R. W.; Chen, X. G.; Lemmon, D. H.; Cho, N.; Peterson, P.; Arrigoni, M.; Spinelli, L.; Cannon, J. *Applied Spectrosc.* **1993**, *47*, 628−633. (c) Asher, S. A. *Anal. Chem*. **1993**, *65*, 59, 201.
(22) Wang, T. S. C.; Huang, P. M.; Chou, C. H.; Chen, J. H In *The role of soil minerals in the abiotic polymerization of phenolic compounds and formation of humic substances*; Huang, M., Schnitzer, M., Eds.; 1986.
(23) Welhouse, G. J.; Bleam, W. F. *Environ. Sci. Technol.* **1993**, *27*, 494.
(24) Stern, M. K.; Groves, J. T. In *Manganese Redox Enzymes*; Pecoraro, V. L., Ed.; VCH Publishers: 1992; pp 233−259.

Received for review April 13, 1999. Revised manuscript received June 28, 1999. Accepted July 1, 1999.

ES990419T